Magazine of Civil Engineering. 2019. 87(3). Pp. 3–17
Инженерно-строительный журнал. 2019. № 3(87). С. 3–17

Magazine of Civil Engineering

ISSN 2071-0305

journal homepage: http://engstroy.spbstu.ru/

DOI: 10.18720/MCE.87.1

The geometric shape effect of steel slit dampers in their behavior

M.A. Kafi*, K.Nik-Hoosh
Semnan University, Semnan, Iran
** E-mail: mkafi@semnan.ac.ir*

Keywords: yield damper; cyclic loading; flexural behavior; shear behavior; dissipated energy

Abstract. Dampers are excellent for improving the performance of steel structures and protecting them against earthquakes. The Steel Slit Damper (SSD) is a type of damper designed to be replaced after being damaged under a strong earthquake. Aiming to investigate the effects of the number of blade rows and optimize the length-to-width ratio of blades, seven specimens of identical thickness with one or two rows of blades and three length-to-width ratios were tested and subjected to static cyclic loading. Different parameters, including the force capacity, displacement capacity, effective stiffness, dissipated energy, ductility, and damage indices, were calculated from the experimental results and compared. The results indicate the evident advantage of dampers with two rows of blades in terms of the force capacity, effective stiffness, and absorbed energy, as the highest force capacities corresponding to the two groups exhibited a 61.6 % difference. Furthermore, given the advantage of dampers with two rows of blades and based on the observations, an optimal blade length-to-width ratio (h/b) of 1.58 is recommended to prevent buckling.

1. Introduction

In recent decades, the use of energy dissipation systems experienced rapid growth in construction. Such systems can be generally categorized into active, passive, semi-active, and hybrid groups. Among the said dampers, the passive damper does not require an external source of energy. Unlike common methods of designing earthquake-resistant structures that absorb most of the seismic energy by yielding at certain points (typically at the ends of beams and columns in the moment frame system), in passive control systems, the energy is dissipated by certain devices known as seismic dampers. These systems offer several advantages, including (1) absorbing non-elastic deformations – thus allowing for a considerable reduction of damages to the main structure; (2) reducing the lateral structural displacements that, for its part, limits the damage to non-structural components, and (3) facility of inspection, repair, and replacement without requiring the evacuation of the building [1]. As shown in Figure 1 several Steel Slit Dampers (SSDs) – including the ADAS [2], TADAS [3], and the double X-shaped [4] – have been proposed as passive control systems.

Chan et al. [5] introduced the SSD for the first time in a study on the effect of slits in three different configurations. In their study on these dampers, Teruna et al. [6] showed that slits with convex edges prevent low cycle fatigue and are far more stable under cyclic loading. In another study, the effect of the slit was investigated against variable height, concluding that a configuration with thinner blades in the middle and thicker ones on the sides improves energy dissipation to some extent under cyclic loading [7]. The effect of different slits shapes (blades or bands with variable cross-section) was also investigated, showing that dumbbell-shaped, gradually-narrowing blades offer a better earthquake performance [8]. A study on this type of damper addressed dampers with variable cross-section and (fixed) large thickness. Given the large thickness of their bands, such dampers are resistant to buckling. The said study investigated the optimal aspect ratio for damper blades [9].

Kafi, M.A., Nik-Hoosh, K. The geometric shape effect of steel slit dampers in their behavior. Magazine of Civil Engineering. 2019. 87(3). Pp. 3–17. DOI: 10.18720/MCE.87.1.

Кафя М.А., Ник-Хуш К. Влияние геометрической формы распределительных клапанов на их характеристики // Инженерно-строительный журнал. 2019. № 3(87). С. 3–17. DOI: 10.18720/MCE.87.1.

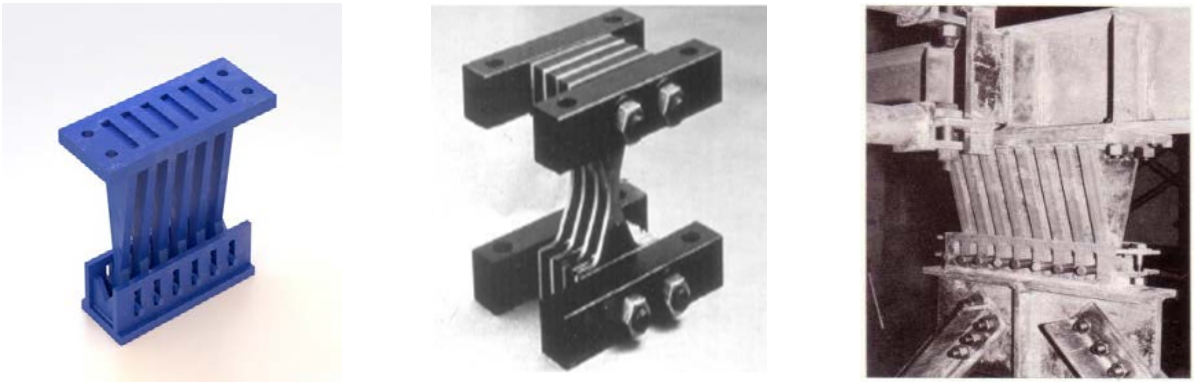

(a) **(b)** **(c)**

Figure 1. a) TADAS damper b) double X-shaped damper c) TDAS damper.

This type of damper is employed in both bracing (Figure 2a) and beam-to-column (Figure 2b) connections. These dampers are placed in the frame such a way that reach to yield strength due to shear, bending or axial force. In order to dissipate energy, it is necessary to consider how to embed them in a frame to undergo deformation due to the relative displacement of the floor which caused by the lateral load; otherwise, they will not function and dissipate energy properly.

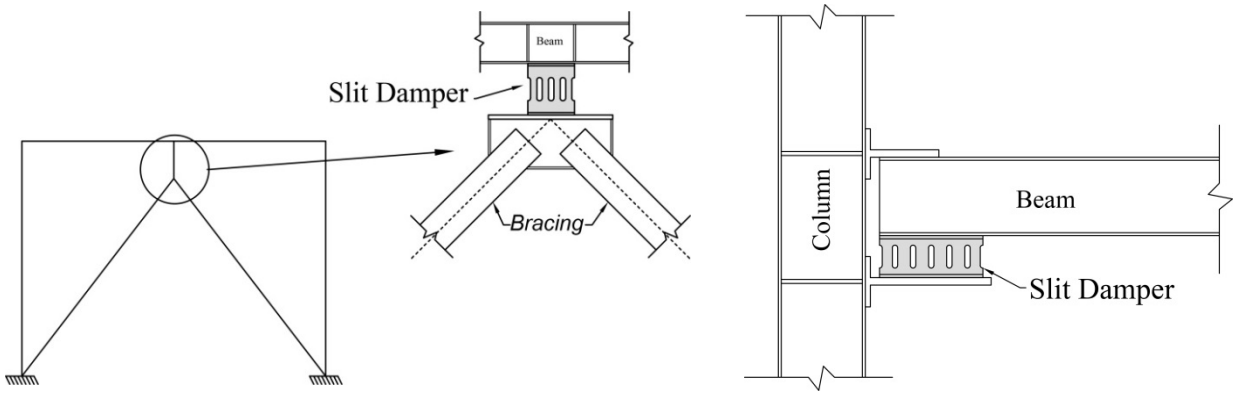

(a) **(b)**

Figure 2. Different uses of the SSD a) Integration into bracing connection and b) Integration into beam-to-column connection.

Lin et al. [10] developed a buckling-restrained damper with a replaceable, composite, steel – concrete shear plate protection. Twelve specimens were tested in order to investigate effective design parameters such as the type of steel, the number of internal panels, etc. on the seismic behavior of dampers. Furthermore, relations were suggested to estimate the elastic stiffness and the ultimate strength of the dampers. Xu et al. [11] investigated four types of shear panel dampers by cyclic tests using a new type of low-yield-strength steel (BLY160) to study the seismic behavior. Chaofeng et al. [12] developed a model of the hysteretic mechanical characteristics of low-yield-strength shear panel dampers under extreme plastic deformation and verified it using other models and experimentally testing the dampers. In another study, the authors addressed low-cycle fatigue in small shear panel dampers made of low-yield-strength steel under monotonic and cyclic loading [13]. They also investigated the possibility of predicting the performance of shear panel dampers using finite-element software, claiming this approach to be useful as regards this type of damper [14]. Chen et al. [15] made an attempt at the numerical simulation of large deformations in Shear Panel Dampers (SPD) by the Smoothed-Particle Hydrodynamics (SPH) method. Shen et al. [16] analytically investigated the seismic behavior of concentrically braced frames with and without brace buckling. Given the dependence of the performance of Steel Shear Panel Dampers (SSPD) on the stiffener arrangement and the type of steel, Deng et al. [17] addressed the optimization of the shapes of these dampers aiming to improve their low-cycle fatigue performance. Moreover, in a study, the authors proposed a method for designing buckling plates in buckling-restrained SPDs by examining five test dampers, evaluating their experimental results using ABAQUS. Bazzaz et al. [18] proposed and evaluated the new bracing system using nonlinear software. Andalib et al. [19] experimentally investigated three types of steel rings and their ductility in bracing frames they also performed a finite element study using ANSYS software. Latour et al. [20] made an attempt at the experimental and numerical investigation of two types of friction dampers in beam-to-column metallic connections that can limit structural damages inflicted by severe seismic conditions. Their experimental and numerical results verified the effectiveness of this type of damper, offering a considerable improvement in design requirements. Zeynali

et al. [21] used lead rubber damper which was constructed with steel core and rubber plates in chevron concentrically braced frames and studied their behavior experimentally and numerically.

Qu et al. [22] studied a new type of seismic dampers with replaceable U-shaped metal plates. Their study involved seven experimental specimens, reporting that all specimens exhibited stable hysteretic performance and excellent capacity for energy dissipation. Furthermore, replacing the damaged U-shaped metal plates led to favorable results under consecutive loading. Furthermore, relations were presented to estimate the yield strength and the ultimate strength of the dampers. Sahoo et al. [23] carried out an experimental investigation of the shear-and-flexural metallic yielding dampers under cyclic loading. The tested dampers included two types of plates that yielded under shear or flexural loading. The plate dimensions varied in this study and covered different parameters including the load-bearing capacity, energy dissipation, and ductility. Furthermore, a numerical study was carried out, delineating a design process.

According to previous studies, in the present study, focusing on steel slit dampers, the effect of geometric characteristics and blade arrangement, and the relative dimensions of gaps with constant cross-section and fixed thickness on cyclic behavior and hysteresis curves are studied. According to the results of experimental tests on 7 specimens, the effect of the different dimensions on the shear force, ductility, absorbed energy and etc. the most suitable arrangement of the slits and the optimal ratio of geometric dimensions for the dampers are suggested. The most prominent feature of this research is the installation and testing of dampers inside the braced frame in order to approach the behavior of the dampers to the actual conditions and to observe the effect of the frame on their behavior. Also, in this study, with the aim of using a large range of geometrical dimensions of the damper section, beam girder was used to construct dampers.

2. Method

In order to investigate the behavior of slit dampers in braced steel frame under cyclic loading, an experimental method was used. In this section, firstly existing equations for calculation of elastic stiffness, yield force, and yield displacement were presented for slit dampers, and then the specification of experimental specimens were introduced.

2.1. Analytical Relations

Relations are presented in this section for elastic stiffness, force, and the yield displacement of the damper based on the principles of solid mechanics. These relations can be used to design dampers in proportion to the seismic demands.

2.1.1. Elastic Stiffness

Figures 3 and 4 illustrate the behavior of a blade using an equivalent fixed-end beam. The simplified behavior is relevant when the stiffness of the blade is much lower than that of the supports, which considerably simplifies the calculations.

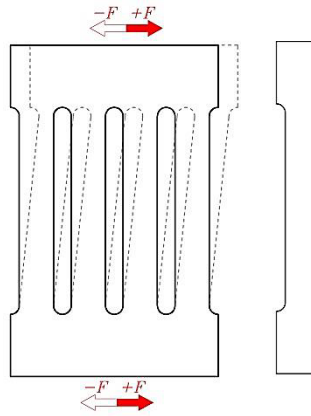

(a) (b)

Figure 3. Schematic view of damper mechanism a) The mode of deflection of SSD b) Blade selected.

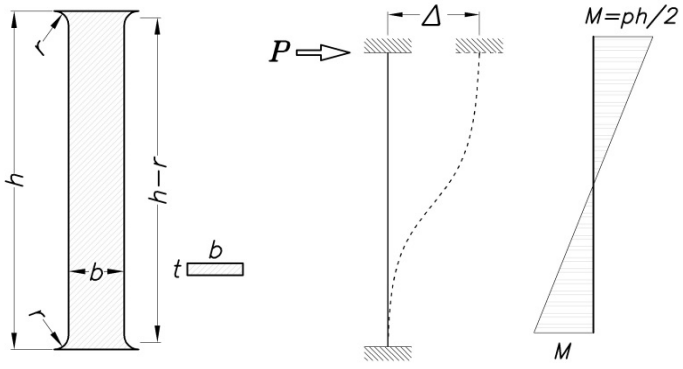

(a) (b) (c)

Figure 4. Blade equivalent to a fixed-end beam a) Blade b) Blade deformation under lateral loading c) Moment diagram.

In dampers with one row of blades, the geometry suggests that this simplified behavior is usable. However, it can be shown for dampers with two rows of blades, that the condition is only satisfied when the h/b ratio (Figure 4) is enough larger than the $2r/c$ (where r is the curvature radius at the end of the blades and $2r$ is the free distance between two blades and c is the distance between two rows in dampers with two rows of blades).

Given the large value of h/b ratio, shear deformation has a significant contribution to the total deformation, which must be taken into account. With the above discussions, the elastic stiffness of a blade can be calculated using Eq. (1).

$$k_1 = \frac{Etb^3}{h^3(1+3b^2/h^2)}, \tag{1}$$

where E represents the elastic modulus of the damper steel, and the parameters corresponding to the geometry of the damper are presented in Figure 4.

The relation ignores the small curvature at the end of the blade, therefore if *r* is smaller than h, it is best to replace h with *h*-*r* when using Eq. (1) to improve the accuracy of results. Knowing the stiffness of a single blade, and given the uniformity across all blades, the elastic stiffness can be calculated for dampers with *n* blades in a single row and $2n$ blades in two rows (two rows of blades in *n* columns) by using Eq. (2) and Eq. (3) respectively.

$$k = nk_1; \tag{2}$$

$$k = \frac{nk_1}{2}. \tag{3}$$

As explained above $2r$ is the free distance between the two blades. Assuming that the damper is similar to a frame, the blades have the role of the columns and middle elements have the role of the beams. Given that, the cross-section of the beams and its columns is rectangular with a constant width *t* (the thickness of the damper), it is obvious that h/b indicates the stiffness of the blades and $2r/c$ represents the softness of the middle elements. If the beams are not hard enough, the plastic hinge is formed in the middle element instead of the blade, which contradicts the initial assumptions so it must be noted that the h/b ratio is more than 4.2 times the $2r/c$, which satisfies the conditions necessary for using the above relations.

2.1.2. Yield Force and Displacement

Assuming the dominance of flexural behavior and formation of plastic hinges at both ends of each blade and by referring to the moment diagram in Figure 4, the yield force of a one- or two-row damper with *n* blade columns under bending can be formulated according to Eq. (4).

$$P_{yb} = \frac{nb^2tf_y}{3h}, \tag{4}$$

where f_y is the yield strength of the damper steel. For dampers with two rows of blades, in case *c* is enough larger than b, the blade yields at both ends, and Eq. (4) remains relevant for calculating the yield force.

Knowing the yield force from Eq. (4) and elastic stiffness from Eqs. 2 or 3, yield displacement can be calculated from Eq. (5).

$$\Delta_y = \frac{P_y}{k}. \tag{5}$$

In case the shape factor of a rectangular cross-section (Z/S = 1.5 where Z is plastic section modulus and S is elastic section modulus for rectangular section) is used, Eq. (6) can be obtained from Eq. (5) to estimate the plastic force of one- or two-row damper with *n* blade columns.

$$P_p = \frac{nb^2tf_y}{2h}. \tag{6}$$

Under the dominance of the shear behavior, the yield force of one- or two-row damper with *n* blade columns for a rectangular cross-section is obtained from Eq. (7).

$$P_{ys} = \frac{2nbtf_y}{3\sqrt{3}}. \tag{7}$$

Depending on the type of the dominant behavior, the yield force and the maximum apparent force of the dampers can be obtained analytically from the following relations [5].

$$P_y = \min\left\{n\frac{f_y tb^2}{3h}, n\frac{2f_y tb}{3\sqrt{3}}\right\}, \quad P_u = \min\left\{n\frac{f_u tb^2}{3h}, n\frac{2f_u tb}{3\sqrt{3}}\right\}. \tag{8}$$

As it was mentioned earlier, the first term in the Eq. (8) was obtained assuming the yield of the damper under bending, whereas in the second term the damper is assumed to yield under shear. In Eq. (8) f_u is the maximum stress. The factor 2/3 in the second term of the above equations responds to the fact that the ratio of the average to maximum shear stresses is 2/3 when the b/h ratio is less than 1 in the elastic range.

2.1.3. Slit Damper Analysis Mechanism

The second moment of area *I* is calculated from the prismatic geometry of the blades [5].

$$I = tb^3/12. \tag{9}$$

When the moment is large enough, the bending moment at the end of the blades brings the farthest fibers to the yield stress. As a result, plastic hinges form at both ends by rotation θ_p. For geometrical beams, the full plastic moment M_p is obtained using the following relation:

$$M_p = f_y \frac{tb^2}{4}. \tag{10}$$

The ultimate damper force can be calculated based on the failure mechanism when the entire ultimate moment of the beam is used up in a plastic hinge. Based on conservation of energy, and assuming full elastic-plastic behavior for the materials, the following equation is obtained.

$$P_y \delta_p = 2nM_p \theta_p. \tag{11}$$

Using the geometrical relations of Figure 5 the plastic displacement that the damper can withstand can be expressed in terms of plastic rotation as follows [5]:

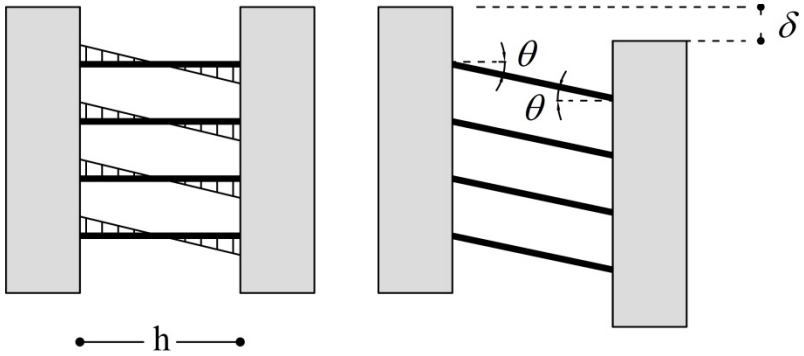

Figure 5. a) Bending moment in the single-row damper; b) the deformed single-row damper.

$$\delta_p = h \tan \theta_p. \tag{12}$$

For small rotations where $\tan \theta_p \approx \theta_p$ Eq. (12) can be rewritten as follows:

$$\delta_p = h\theta_p. \tag{13}$$

By replacing Eqs. 10 and 13, Eq. (11) can be rewritten as follows:

$$P_y = \frac{2nM_p}{h} = \frac{nf_y tb^2}{2h}. \tag{14}$$

In order to investigate the behavior of slit dampers in braced steel frame under cyclic loading, an experimental method was used.

2.2. Specimen Details

In order to achieve the study objectives (investigate the geometric characteristics and blade arrangement, observe the effect of the frame on SDD's behavior) seven experimental specimens were made and tested. Three simple slit specimens with a single row of four uniform blades, three specimens with four uniform blades in two rows, and a no-slit one – the reference – were tested. The blade height (h) was assumed as the variable whereas the thickness (t) and width (b) of the blades were fixed. Accordingly, besides investigating the rows of dampers, the dimensionless h/b ratio of the blades was also discussed as the main variable of the parametric study. Figure 6 illustrates the details of the slits and the dimensions of the specimens DFF, DSSH, DSDH and also a real specimen of DSDH before the test. The geometrical parameters illustrated in Figure 6 are presented in Tables 1 and 2 for specimens with one and two rows of slits, respectively.

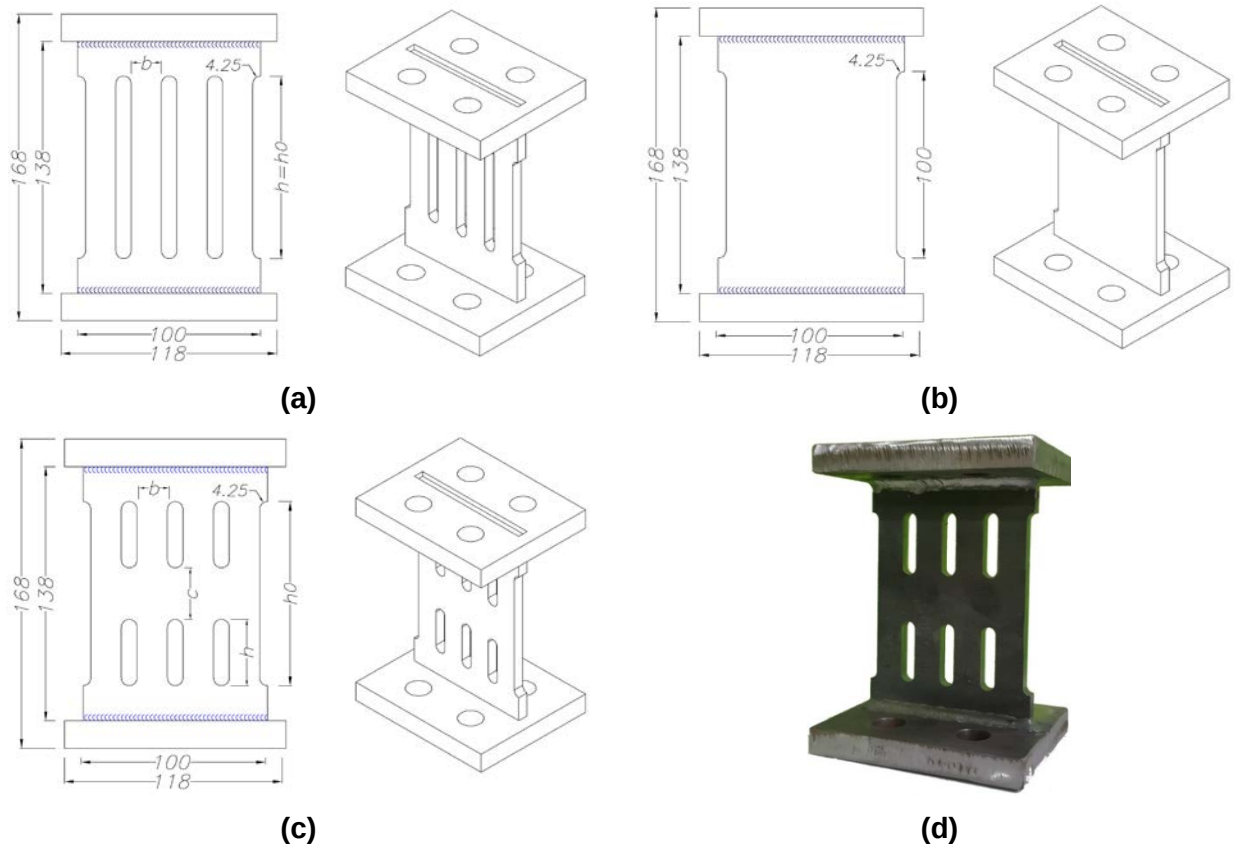

Figure 6. The geometry and parameters determining the specifications of the specimens (all sizes are in mm) a) DSSH b) DFF c) DSDH d) DSDH before the test.

Table 1. The geometrical specifications (mm) of the specimens with one row of blades.

Specimen	h/b	$h_0 = h$	b	t
DSSH1	4.85	80	16.5	8
DSSH2	5.45	90	16.5	8
DSSH3	6.06	100	16.5	8

Table 2. The geometrical specifications (mm) of the specimens with two rows of blades.

Specimen	h/b	c	h	h_0	b	t
DSDH1	1.28	28	21	80	16.5	8
DSDH2	1.58	28	26	90	16.5	8
DSDH3	1.88	28	31	100	16.5	8

2.3. Material Specifications

Table 3 presents the mechanical specifications of the steel used to make a prism specimen with 2.7 in 6 mm^2 rectangular cross-section obtained by standard tensile testing [24]. St 37 steel plate is in DIN 17100 standard.

Table 3. Steel Properties.

Specimen	Maximum strain	Ultimate strength N/mm^2	Yield strength N/mm^2
St 37	0.4	434	250

2.4. The Arrangement and Laboratory Equipment

In order to establish real conditions and investigate the behavior of the damper inside the frame, the specimens were installed on a chevron brace (Figures 7 and 8). As a general rule in the design of the frame and braces, these elements were calculated so that the frame and braces remain in the elastic behavior zone when the damper is in the plastic zone under cyclic loading. Accordingly, the maximum force capacity of the dampers, which was related to the DFF specimen, was calculated and with the obtained capacity, the structural calculations and frame elements including the beam, column, braid and connection sheets were done. The specimens were attached to the braces at the bottom and to the rigid beam at the top and then tested. To prevent the rotation of the rigid beam (simulating a rigid ceiling) and the displacement of the loading jack and the rigid beam in a linear path, and to restrict their out-of-plane movements, the rigid beam was connected to a Linear Motion Guide (LMguide) at the top. Furthermore, given that the beam-column connection is a hinge, the connection was removed by simulating the equivalent frame behavior.

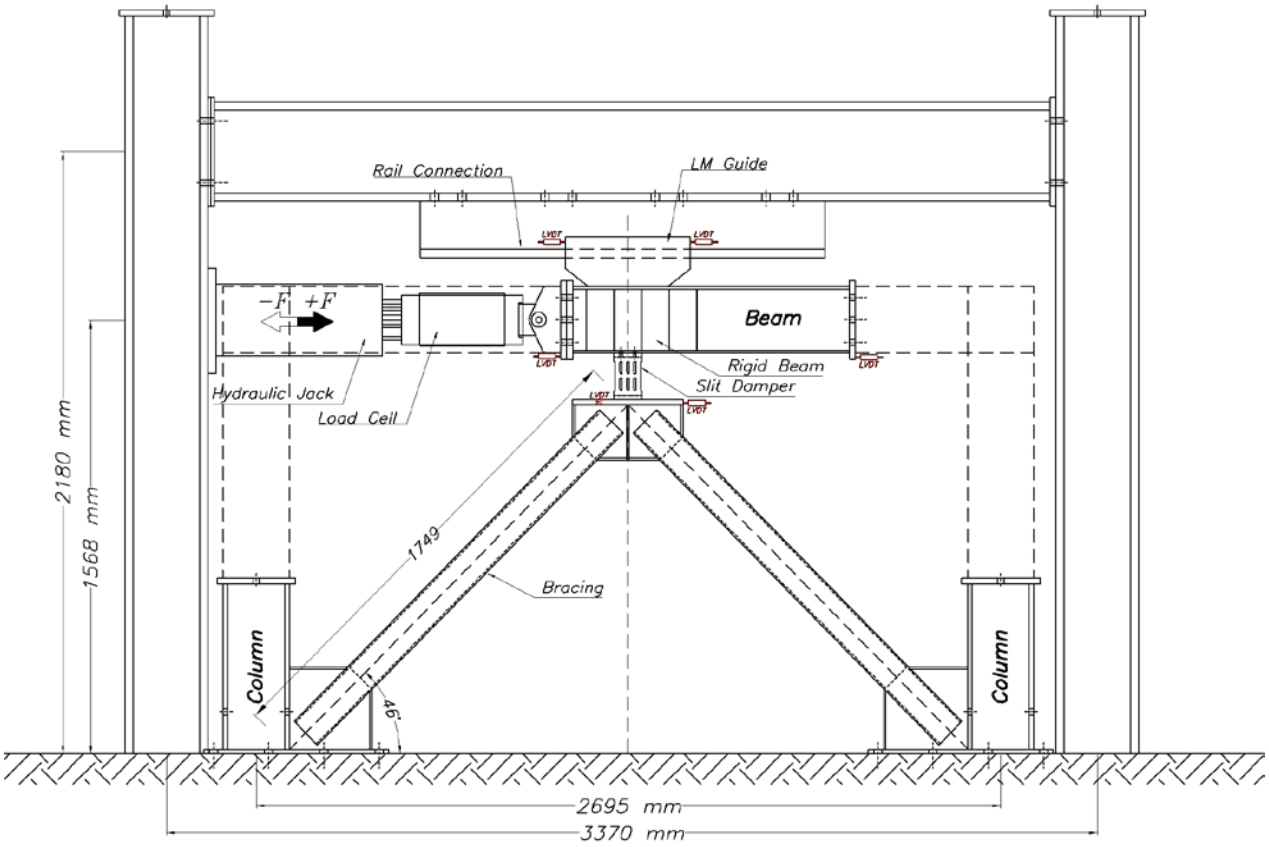

Figure 7. Test layout design for cyclic loading.

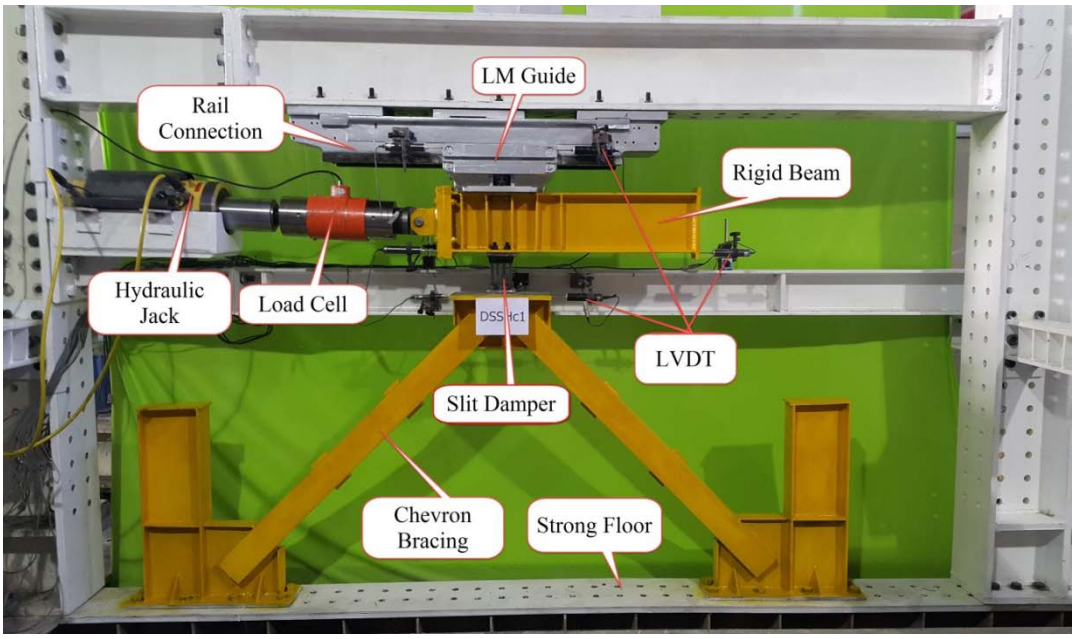

Figure 8. Test layout system and the installations.

A hydraulic jack with 100 ton capacity in tension and 200 ton in compression was used to test the specimens. Furthermore, a 100-ton tension/compression load cell was employed to measure the force exerted on the specimen. Four 4 cm LVDT units were used to record the specimen displacements. Moreover, three LVDT units were also placed on the brace plates to investigate in-plane and off-plane movements. The test layout and the equipment are illustrated in Figures 7 and 8. Furthermore, Figure 9 shows the LMguide layout and the exact location of the LVDT units.

The specimens were subjected to static, cyclic loading according to the test plan. The loading process was displacement controlled. An incremental loading history based on the ATC-24 protocol [25] was used to apply the said loading cycle. Figure 10 illustrates the loading protocol applied to the specimen. In this protocol, each displacement is applied to the specimen three times back and forth, continuing until it is destroyed.

Figure 9. The LMguide and the location of the LVDT units.

2.5. Test Plan and Layout

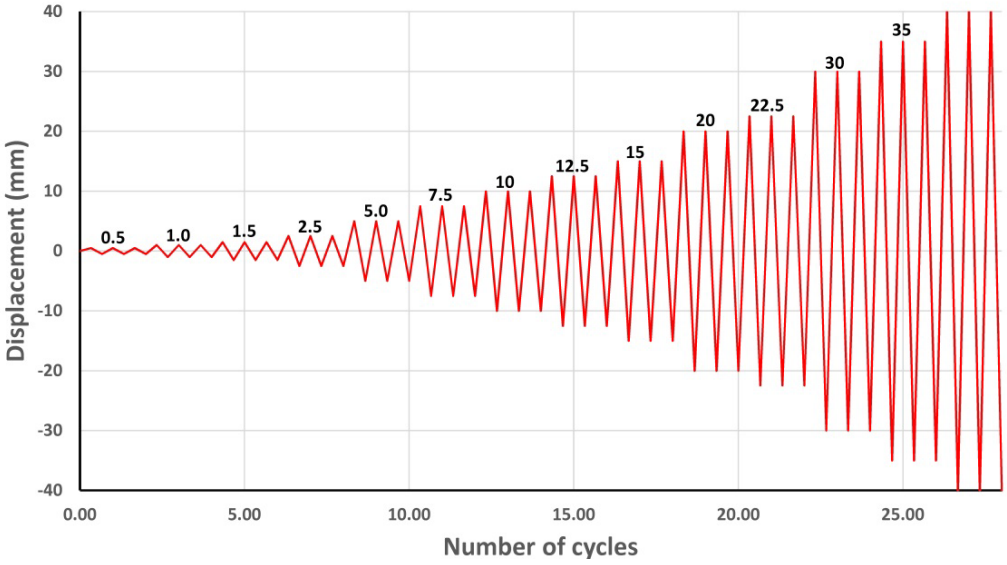

Figure 10. The incremental cyclic loading history [25].

3. Results and Discussion

In this section, after presenting the outputs of the experimental study, the results are reviewed, compared, and analyzed. The said outputs include cyclic behavior, effective stiffness, dissipated energy, and equivalent viscous damping. Furthermore, a damage index was also calculated and presented for the specimens.

3.1. The Cyclic Behavior of the Specimens

The specimens were tested by static cyclic loading according to the scheme presented in Figure 10, recording the force variations, displacements, and other parameters. The resulting cyclic diagrams under the said loading are presented in Figure 11 Moreover, Figure 12 presents the envelope curve of the specimens. The envelope curve is plotted by specifying the maximum force endured in every three cycles (equal displacements) and connecting the maximum points obtained for the cycles.

Table 4 presents the maximum force and maximum displacement results, representing the force and displacement capacities of each specimen. The maximum displacement corresponds to a force that does not exhibit a drop of over 20 % relative to the maximum force.

It is safe to conclude from Table 4 that the load-bearing capacity of the specimens increases by reducing the h/b ratio (the blade height) and increasing blade rows from one to two. A comparison of the maximum displacement of the specimens shows it to decrease by adding to the number of blade rows. It must be noted that reducing the h/b ratio translates into the dominance of the shear behavior over the flexural behavior in the blades. In specimens with identical number of blade rows, DSSH2 and DSDH2, exhibiting 40 and 1.9 % improvements relative to the reference specimen, correspond to the highest displacement capacities, whereas DSSH1 and DSDH1, with 17.58 % increase and 16 % reduction in comparison to the reference specimen, showed the smallest displacement capacities in each group. Generally speaking, an increase in the h/b ratio increases the maximum displacement, however, the increase is the largest in a certain range. Figure 13 illustrates the deformed DSSH1 and DSDH1 at their respective maximum force capacities.

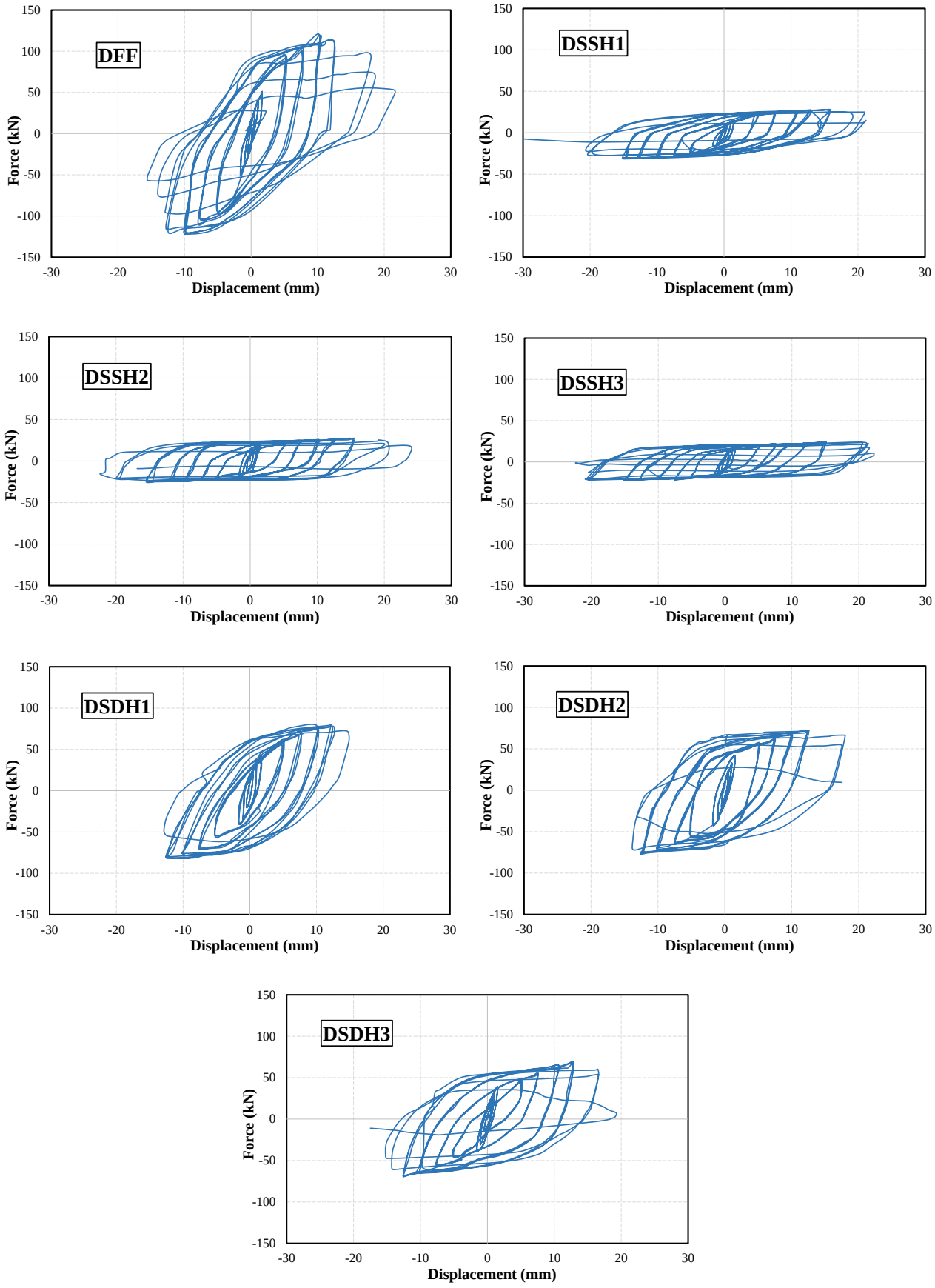

Figure 11. The cyclic force-displacement behavior of the specimens.

Given the fact that the two specimens (DSSH1 and DSDH1) correspond to the smallest h/b ratios in their respective groups, they offered the largest load-bearing capacities. The deformation of the specimens shows that yield takes place inside the blade and the outside region is not affected much, which verifies the assumptions made to simplify the analytical relations.

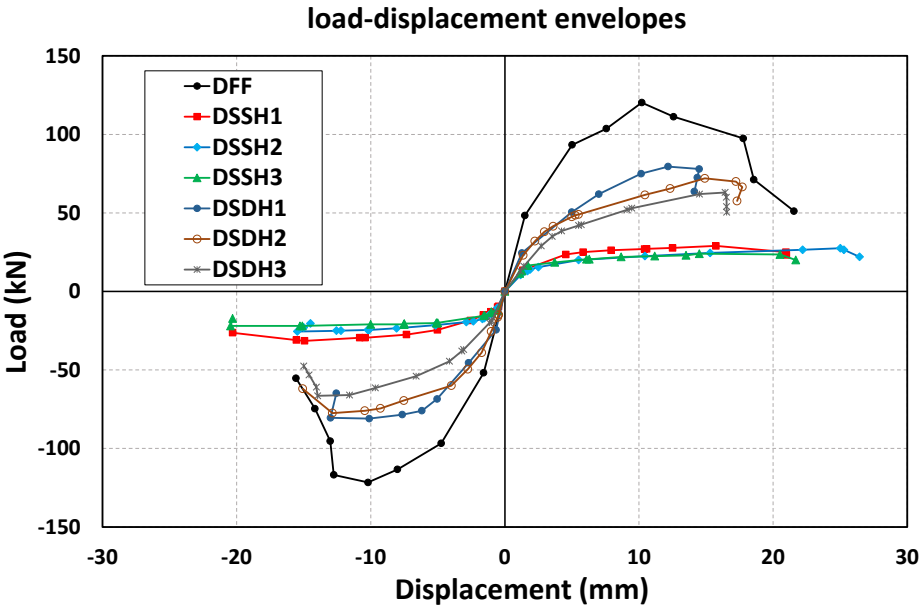

Figure 12. The envelope curves of the tested specimens.

Table 4. Maximum force and displacement in the specimens.

Specimen	*b*	*t*	*h*	*c*	Maximum Force (kN)	Maximum Displacement (mm)
DFF	100	8	100	---	118	17.86
DSSH1	16.5	8	80	---	31.5	21
DSSH2	16.5	8	90	---	27.5	25
DSSH3	16.5	8	100	---	25	21.3
DSDH1	16.5	8	26	28	82	15
DSDH2	16.5	8	31	28	77.5	18.2
DSDH3	16.5	8	36	28	66.5	16.7

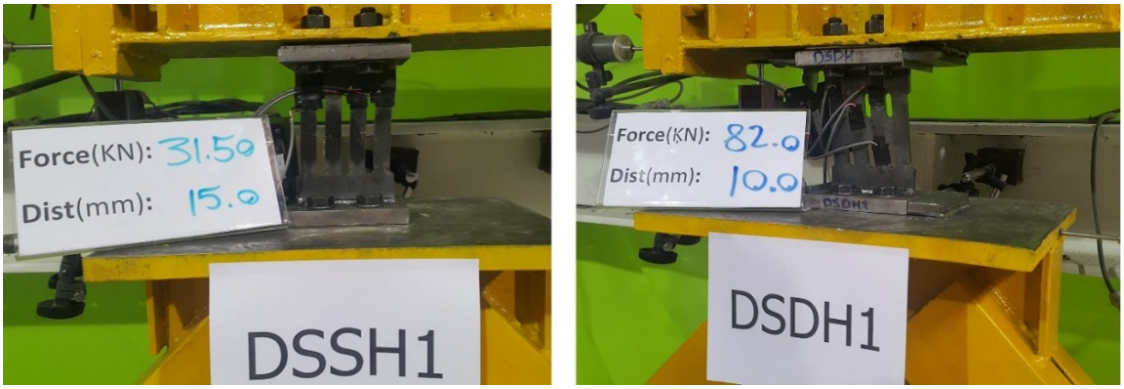

Figure 13. The deformation of DSSH1 and DSDH1 at maximum force.

3.2. Effective Stiffness

The elastic potential energy of the damper can be calculated in each cycle using the effective stiffness. This energy tends to restore the damper to its initial conditions. It is evident that, with the damper entering the plastic phase, the energy is not sufficient to restore the damper and is mostly supplied by the exerted external force. The elastic potential energy and the energy dissipated in one cycle are presented in Figure 14 The effective stiffness $(K_{i,eff})$ can be calculated using Eq. (15).

$$K_{i,eff} = \frac{\left(\left|P^{+}_{i,max}\right| + \left|P^{-}_{i,max}\right|\right)}{\left(\left|\delta^{+}_{i,max}\right| + \left|\delta^{-}_{i,max}\right|\right)}. \quad (15)$$

All parameters in this relation are defined and illustrated in Figure 14.

Figure 15 plots the changes in the effective stiffness of the specimens against displacement. According to Eq. (15), the higher the force endured at a small displacement, the higher the effective stiffness of the specimen. The changes in the effective stiffness curve indicate it to be large at small displacements but to decrease drastically to a fixed level by increasing the displacement.

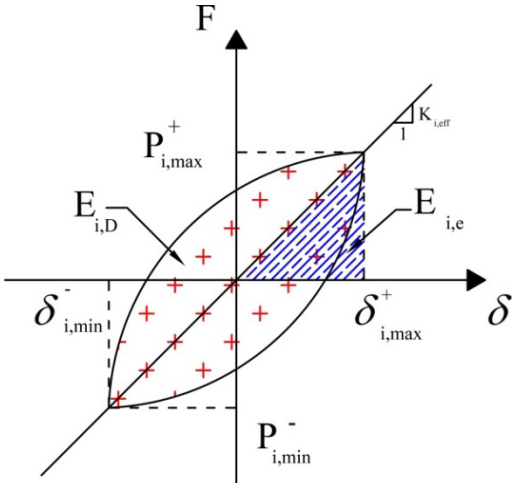

Figure 14. The effective stiffness and the cyclic energy in cyclic loading [9].

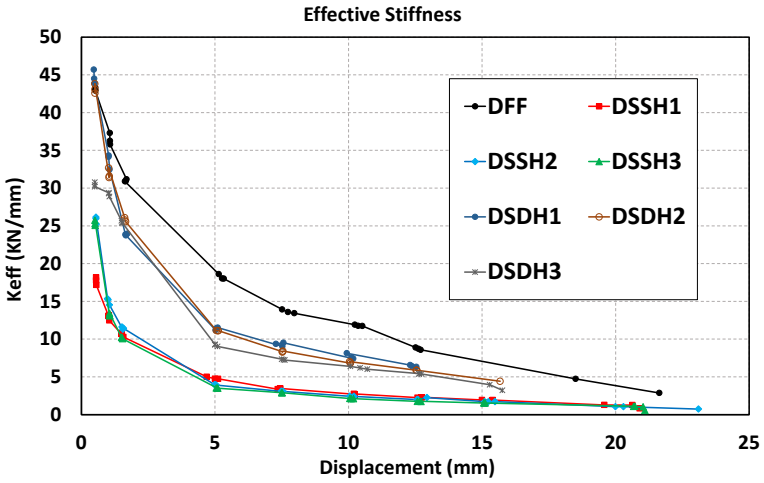

Figure 15. Effective Stiffness of the Specimens.

Figure 15 indicates the reference specimen to correspond to the highest effective stiffness, as well as initial stiffness, followed by the specimens with two rows of blades and those with one row of blades. Equation 15 shows that the double-row specimens exhibited a higher stiffness than the single-row ones for the same displacement. Specimens with a similar number of blades were found to be similar in terms of stiffness, however, it is safe to say that, in general, the effective stiffness is reduced by increasing the h/b ratio. The behavior of the specimens is also suggestive of that the effective stiffness difference between the specimens is rapidly reduced by further increasing the displacement. A comparison of the diagrams shows the rate of decrease of the effective stiffness is much higher in specimens with two rows of blades (DSDH with dominant shear behavior) than in those with a single row of blades (DSSH with dominant flexural behavior). It is evident that the high softening rate (drastic drop in stiffness) is not favorable in structures and promotes the formation of a soft story.

3.3. Dissipated Energy and Equivalent Viscous Damping

Dissipated energy is the hysteresis area in cyclic loading. The dissipated energy was calculated for all specimens for different displacements as illustrated in Figure 16 together with the cumulative dissipated energy. The curves suggest that specimens with two rows of blades (DSDH) are much stronger energy dissipators than those with a single row. In other words, it can be said that the dissipated energy increases under the dominance of shear behavior. In specimens with two rows of blades, energy absorption increases at larger h/b ratios, however, DSDH2 exhibited the highest energy absorption among single-row specimens, whereas the other two specimens were similar in their performance.

The observation of these curves, on the other hand, indicates that the tendency of the samples to the shear behavior can reduce the displacement capacity and increase the energy absorption of them.

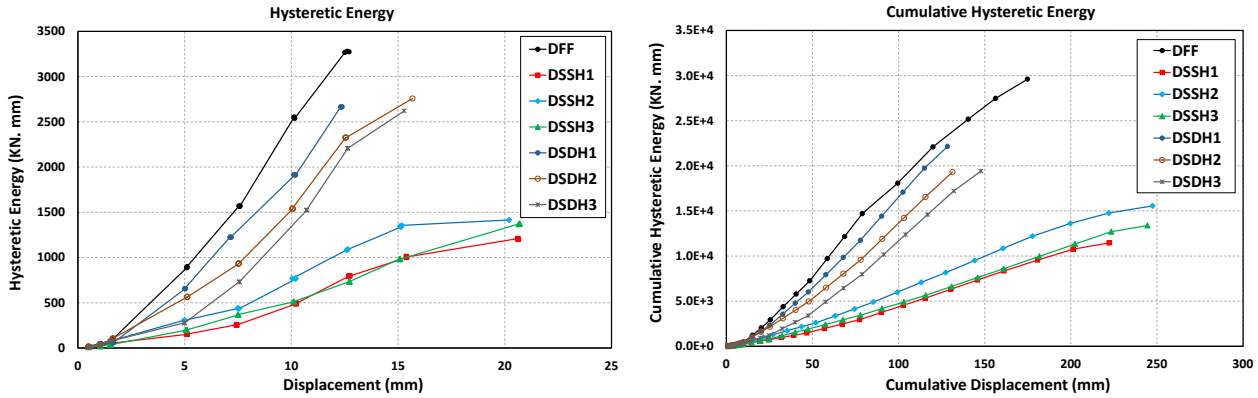

(a) **(b)**

Figure 16. a) The energy dissipated in each cycle; b) cumulative energy dissipation.

Figure 17 plots the equivalent viscous damping against displacement for each damper. The equivalent viscous damping or effective damping – that equates the behavior of a nonlinear system to a linear one with viscous damping – represents, in fact, the ratio of dissipated energy to elastic potential energy resulting from

secant stiffness at maximum displacement (effective stiffness) in each cycle. The effective damping can be calculated from Eq. (16) according to Figure 14 [26].

$$\beta_{i,eff} = \frac{E_{i,D}}{4\pi E_{i,e}} = \frac{2E_{i,D}}{\pi K_{i,eff}\left(\left|\delta^{+}_{i,max}\right| + \left|\delta^{-}_{i,max}\right|\right)^2} \tag{16}$$

where $\beta_{i,eff}$ represents effective damping in the I the cycle. The other parameters in this relation were defined and illustrated earlier in Figure 14.

According to Figure 17, illustrating the cumulative damping in different displacements for all specimens, it can be said that, overall, single-row specimens are better dampers than their double-row counterparts. Furthermore, in specimens with a similar number of blade rows, those with a larger h/b ratio have a higher equivalent viscous damping, suggesting that the dominance of the flexural behavior increases effective damping.

It must be noted that, given the fact that effective stiffness, or equivalent viscous damping, is obtained by equating a nonlinear system to a linear one, a large effective stiffness is not an advantage to the system on its own. In other words, the required effective stiffness must be evaluated based on the seismic demand of the structure (according to Eq. (16), effective stiffness contributes to this parameter) and its effective stiffness.

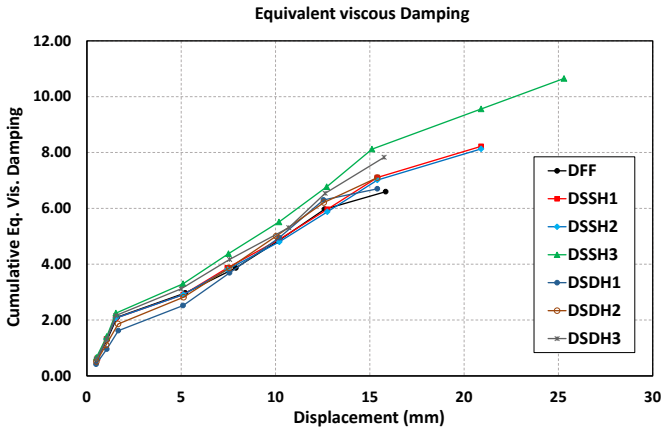

Figure 17. The cumulative effective damping (equivalent viscous damping).

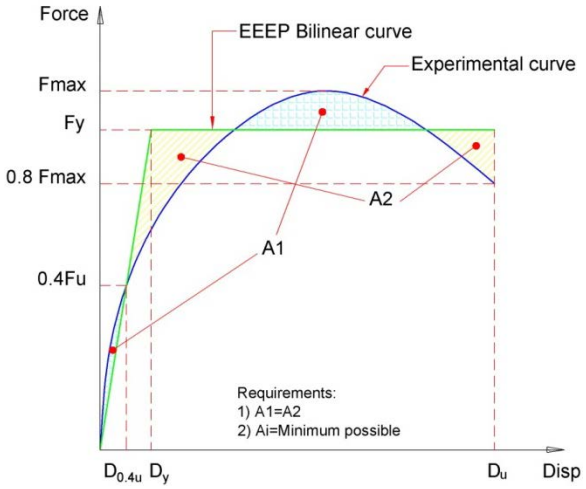

Figure 18. Using the Equivalent Energy Elastic–Plastic (EEEP) bilinear model [27].

3.4. Ductility

Various models have been proposed for modeling ductility, including the Equivalent Energy Elastic–Plastic (EEEP) bilinear model – that is based on the ASTM E2126-09 standard [27] – which was used in this study. Figure 18 presents a detailed illustration of the method. The model assumes a damper system with ideal elastic-plastic behavior, which is capable of dissipating as much energy as in the real damper by equating the areas A1 and A2. The elastic displacement, ultimate displacement, and ductility of all specimens are presented in Table 5. The ductility ratio in specimens (ultimate to yield displacement ratio) is calculated using Eq. (17).

$$\mu = \frac{Ultimate\ \ displacement}{Yield\ \ displacement} = \frac{\Delta u}{\Delta y}. \tag{17}$$

Table 5. Ductility calculations.

Specimen	Elastic Displacement (mm)	Maximum Displacement (mm)	Ductility μ	$\frac{\mu}{\mu_{DFF}}$
DFF	4.983	17.86	3.58	1
DSSH1	2.489	21	8.44	2.36
DSSH2	2.709	25	9.23	2.58
DSSH3	2.482	21.3	8.58	2.4
DSDH1	3.555	15	4.22	1.178
DSDH2	4.304	18.2	4.23	1.181
DSDH3	4.531	16.7	3.68	1.03

Based on the results, it can be inferred that the specimens with a single row of blades feature a higher ductility than the others. Among specimens with one and two rows of blades, DSSH2 and DSDH2 have the highest ductilities, which are 2.58 and 1.181 times the reference. It can be said that the more flexural the behavior of the specimen, the higher the ductility.

3.5. Damage Index

Several damage indices have been proposed by researchers. The indices are quantitative illustrations of the extent of damage to specimens at different displacements. The index measures damage on a scale of 0 to 1, with 0 indicating no damage and 1 suggesting destruction. It is safe to say that the combined damage index, for taking into account the displacement, force, and energy, is the best one, which was used in this study. The index was first proposed in 1985 by Park and Ang [28] and has been used in several experimental works ever since [29, 30].

$$D = \frac{\delta_m}{\delta_u} + \beta \frac{\int dE}{f_y \delta_u}, \tag{18}$$

where δ_m and δ_u are the maximum displacement endured by the specimen under cyclic displacement and the displacement capacity of the specimen, f_y is the yield force, dE is the cyclic energy increment, and β is a constant.

The damage curves of the tested specimens were obtained and presented in Figure 19.

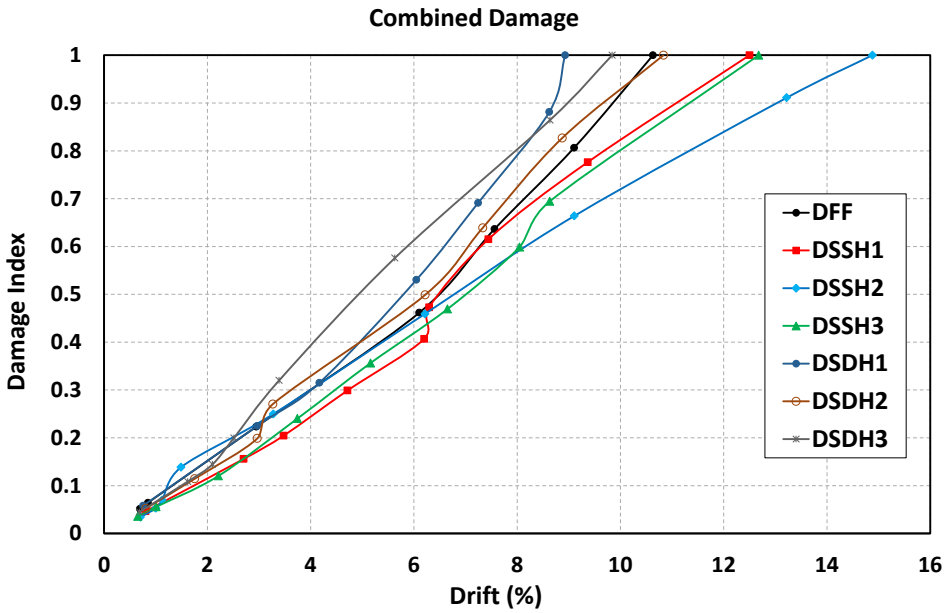

Figure 19. The Calculated Combined Damage Index.

The slope of the line representing the damage index indicates the rate of damage to the corresponding specimen. The figure shows that specimens with two rows of blades have a steeper slope than those with a single row, suggesting faster damage and destruction. Among specimens with a similar number of blade rows, DSSH2 and DSDH2 with h/b ratios of 5.45 and 1.58 have a more gradual slope and, therefore, a lower rate of damage. Furthermore, DSSH1 and DSDH1 – that correspond to the lowest h/b ratios of their respective groups – feature the highest rate of damage.

3.6. Buckling and the Optimal h/b ratio

As it was mentioned in previous sections, a reduction in the h/b ratio promotes shear behavior in the damper, paving way for a favorable performance. Given that a reduction in the h/b ratio increases the damper stiffness, an overall buckling before the damper reaches its maximum capacity becomes more likely. It is, therefore, safe to say that reducing the h/b is allowable and optimal to the extent it does not result in the overall or lateral buckling of the damper. The DFF (h/b = 1.09) and DSDH1 (h/b = 1.28) had the lowest h/b among the studied specimens. Given the fact that the occurrence of overall buckling depends on the slenderness, the h_0/t ratio can be considered as the slenderness ratio. Figure 20 illustrates the overall buckling of DSDH1.

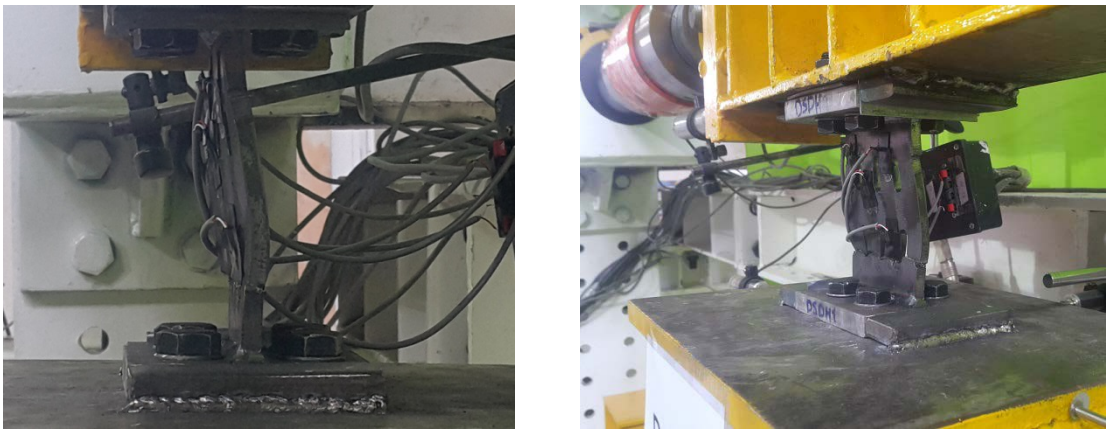

Figure 20. Overall buckling in DSDH1.

The slenderness ratio (h_0/t) was calculated at 12.5 and 10 for the two specimens. Given that overall buckling took place in the said specimens under the applied cyclic loading, the minimum h/b was proposed to be 1.58 (for DSDH2 with a slenderness ratio of h_0/t = 11.25). Assuming a linear buckling between h_0/t and h/b, proportions can be used at other h_0/t ratios; meaning that, if h_0/t doubles, the minimum recommended h/b also increases twofold. However, new theoretical analyses, numerical models, or experimental studies are recommended for other h/t ratios.

4. Conclusion

Steel slit dampers with one and two rows of blades of different length-to-width (h/b) ratios were experimentally studied. The specimens were subjected to static cyclic loading and the following results were obtained after processing the test results.

1. The initial cyclic loading results suggested that by reducing the length-to-width ratio of the blades and with the rise of shear behavior to dominance, the force capacity of the dampers is increased but their displacement capacity remains relatively unchanged. A similar result was obtained with dampers with two rows of blades in comparison with the single-row ones.

2. A comparison of the specimens showed effective stiffness to drop drastically by increasing the displacement and extending the yield of the steel in dampers with dominant shear behavior. However, the inclination of the damper to flexural behavior reduces the rate of reduction of effective stiffness. This is of great importance as regards preventing the formation of a soft story, the concentration of damage over certain floors, and improving the overall performance of the structure.

3. From the standpoint of energy absorption, dampers with two rows of blades (shear behavior) can be said to have an advantage over the single-row ones (flexural behavior). Moreover, energy absorption is promoted by reducing the h/b ratio.

4. A parametric study with varying effective damping shows that effective damping is reduced in the damper with the rise of shear behavior to dominance. In both groups (one and two rows of blades), dampers with the highest length-to-width (h/b) ratios exhibited the highest damping.

5. Observations of the ductility indicated that dampers with a single row of blades have a higher ductility than those with two rows of blades due to their larger displacement capacity.

6. Analyzing the damage index, it was found that specimens with a single row of blades have a smaller rate of damage. In each group, the first specimens (smallest h/b) have the highest rate of damage, but the second ones (medium h/b) feature the lowest rate.

7. The damper stiffness is increased by reducing the length-to-width ratio of the blade, which can result in the overall buckling of the damper and failing to attain the maximum capacity. The optimal recommended length-to-width ratio for the blade depends on the height-to-thickness ratio of the damper, which is a measure of the damper slenderness. For a h_0/t = 11.25 slenderness ratio, a length-to-width ratio h/b = 1.58 was recommended for the blade.

Considering the compared parameters in all specimens and considering that the specimens with shear behavior showed a better and more significant performance in parameters such as force strength, effective stiffness and absorbed energy, as well as considering the absence of buckling of the specimens in loading, it can be concluded that the use of dual-row dampers with a medium h/b ratio is the best and most optimal choice for using this type of dampers.

References

1. Benavent-Climent, A. A brace-type seismic damper based on yielding the walls of hollow structural sections. 2010. Engineering Structures. 32(4). Pp. 1113–1122. DOI: 10.1016/j.engstruct.2009.12.037
2. Whittaker, A.S., Bertero, V.V., Thompson, C.L., Alonso, L.J. Seismic Testing of Steel Plate Energy Dissipation Devices. Earthquake Spectra. 1991. 7(4). Pp. 563–604. DOI: 10.1193/1.1585644
3. Mohammadi, R.K., Nasri, A., Ghaffary, A. TADAS dampers in very large deformations. International Journal of Steel Structures. 2017. 17(2). Pp. 515–524. DOI: 10.1007/s13296-017-6011-y
4. Li, H.-N., Li, G. Experimental study of structure with «dual function» metallic dampers. Engineering Structures. 2007. 29(8). Pp. 1917–1928. DOI: 10.1016/j.engstruct.2006.10.007
5. Chan, R.W.K., Albermani, F. Experimental study of steel slit damper for passive energy dissipation. Engineering Structures. 2008. 30(4). Pp. 1058–1066. DOI: 10.1016/j.engstruct.2007.07.005
6. Teruna, D.R., Majid, T.A., Budiono, B. Experimental Study of Hysteretic Steel Damper for Energy Dissipation Capacity. Advances in Civil Engineering. 2015. Pp. 1–12. DOI: 10.1155/2015/631726
7. Zheng, J., Li, A., Guo, T. Analytical and experimental study on mild steel dampers with non-uniform vertical slits. Earthquake Engineering and Engineering Vibration. 2015. 14(1). Pp. 111–123. DOI: 10.1007/s11803-015-0010-9
8. Lee, C.-H., Ju, Y.K., Min, J.-K., Lho, S.-H., Kim, S.-D. Non-uniform steel strip dampers subjected to cyclic loadings. Engineering Structures. 2015. Vol. 99. Pp. 192–204. DOI: 10.1016/j.engstruct.2015.04.052
9. Ahmadie Amiri, H., Najafabadi, E.P., Estekanchi, H.E. Experimental and analytical study of Block Slit Damper. 2018. Journal of Constructional Steel Research. Vol. 141. Pp. 167–178. DOI: 10.1016/j.jcsr.2017.11.006
10. Lin, X., Wu, K., Skalomenos, K.A., Lu, L., Zhao, S. Development of a buckling-restrained shear panel damper with demountable steel-concrete composite restrainers. Soil Dynamics and Earthquake Engineering. 2019. Vol. 118. Pp. 221–230. DOI: 10.1016/j.soildyn.2018.12.015
11. Xu, L.-Y., Nie, X., Fan, J.-S. Cyclic behaviour of low-yield-point steel shear panel dampers. Engineering Structures. 2016. Vol. 126. Pp. 391–404. DOI: 10.1016/j.engstruct.2016.08.002
12. Chaofeng, Z., Youchun, W., Longfei, W., Meiping, W. Hysteretic mechanical property of low-yield strength shear panel dampers in ultra-large plastic strain. Engineering Structures. 2017. 148. Pp. 11–22. DOI: 10.1016/j.engstruct.2017.06.028
13. Zhang, C., Zhu, T., Wang, L., Wu, M. Ultra-low cycle fatigue performance evaluation of the miniaturized low yield strength steel shear panel damper. Journal of Constructional Steel Research. 2017. 135. Pp. 277–284. DOI: 10.1016/j.jcsr.2017.05.001
14. Zhang, C., Wang, L., Sun, C., Wu, M. Feasibility of the evaluation of the deformation capacity of the shear panel damper by FEM. 2018. Journal of Constructional Steel Research. 147 pp. 433–443. DOI: 10.1016/j.jcsr.2018.04.033
15. Chen, Z., Dai, Z., Huang, Y., Bian, G. Numerical simulation of large deformation in shear panel dampers using smoothed particle hydrodynamics. Engineering Structures. 2013. 48. Pp. 245–254. DOI: 10.1016/j.engstruct.2012.09.008
16. Shen, J., Seker, O., Akbas, B., Seker, P., Momenzadeh, S., Faytarouni, M. Seismic performance of concentrically braced frames with and without brace buckling. Engineering Structures. 2017. 141. Pp. 461–481. DOI: 10.1016/j.engstruct.2017.03.043
17. Deng, K., Pan, P., Li, W., Xue, Y. Development of a buckling restrained shear panel damper. Journal of Constructional Steel Research. 2015. 106. Pp. 311–321. DOI: 10.1016/j.jcsr.2015.01.004
18. Bazzaz, M., Kafi, M.A., Kheyroddin, A., Andalib, Z., Esmaeili, H. Evaluating the seismic performance of off-center bracing system with circular element in the optimum place. International Journal of Steel Structures. 2014. 14(2). Pp. 293–304. DOI: 10.1007/s13296-014-2009-x
19. Andalib, Z., Kafi, M.A., Kheyroddin, A., Bazzaz, M. Experimental investigation of the ductility and performance of steel rings constructed from plates. Journal of Constructional Steel Research. 2014. 103. Pp. 77–88. DOI: 10.1016/j.jcsr.2014.07.016
20. Latour, M., D'Aniello, M., Zimbru, M., Rizzano, G., Piluso, V., Landolfo, R. Removable friction dampers for low-damage steel beam-to-column joints. Soil Dynamics and Earthquake Engineering. 2018. 115. Pp. 66–81. DOI: 10.1016/j.soildyn.2018.08.002
21. Zeynali, K., Saeed Monir, H., Mirzai, N.M., Hu, J.W. Experimental and numerical investigation of lead-rubber dampers in chevron concentrically braced frames. Archives of Civil and Mechanical Engineering. 2018. 18(1). Pp. 162–178. DOI: 10.1016/j.acme.2017.06.004
22. Qu, B., Dai, C., Qiu, J., Hou, H., Qiu, C. Testing of seismic dampers with replaceable U-shaped steel plates. Engineering Structures. 2019. 179. Pp. 625–639. DOI: 10.1016/j.engstruct.2018.11.016
23. Sahoo, D.R., Singhal, T., Taraithia, S.S., Saini, A. Cyclic behavior of shear-and-flexural yielding metallic dampers. Journal of Constructional Steel Research. 2015. 114. Pp. 247–257. DOI: 10.1016/j.jcsr.2015.08.006
24. ASTME8M-04. Standard Test Methods for Tension Testing of Metallic Materials [Metric] (2008) 2008.
25. ATC-24. Guidelines of Cyclic Seismic Testing on Components For Steel Structures, Applied Technology Council, Redwood City, Calif, USA, 1992. [Online]. URL: https://books.google.com/books?id=hQpZs4k38sEC.
26. Chopra, A.K., Chopra, A.K. Dynamics of structures: theory and applications to earthquake engineering. Prentice Hall Englewood Cliffs, NJ, 1995.
27. ASTM Standard test methods for cyclic (reversed) load test for shear resistance of vertical elements of the lateral force resisting systems for buildings. 2009. E2126-09.
28. Park, Y., Ang, A. Mechanistic Seismic Damage Model for Reinforced Concrete. Journal of Structural Engineering. 1985. 111(4). Pp. 722–739. DOI: 10.1061/(ASCE)0733-9445(1985)111:4(722)
29. Haji, M., Naderpour, H., Kheyroddin, A. Experimental study on influence of proposed FRP-strengthening techniques on RC circular short columns considering different types of damage index. 2019. Composite Structures. 209. Pp. 112–128. DOI: 10.1016/j.compstruct.2018.10.088
30. Promis, G., Ferrier, E., Hamelin, P. Effect of external FRP retrofitting on reinforced concrete short columns for seismic strengthening. Composite Structures. 2009. 88(3). Pp. 367–379. DOI: 10.1016/j.compstruct.2008.04.019

Contacts:

Mohammad Ali Kafi, +982331535206; mkafi@semnan.ac.ir
Kianoosh Nik Hoosh, +982333331100; K.NikHoosh.PHD@semnan.ac.ir